Analysis of coupling effect on twin waveguides defined by ion implanted AlGaAs/GaAs quantum wells

Alex T. H. Li and E. Herbert Li,
Department of Electrical and Electronic Engineering, University of Hong Kong,
Pokfulam Road, Hong Kong

ABSTRACT

An accurate model is presented for the analysis of ion-implanted AlGaAs/GaAs multi-quantum well symmetric and asymmetric twin waveguides. The modal propagation constants, modal indices and field profiles of the leading supermodes are solved numerically by using a quasi-vector method based on the Finite Difference method. Impurity induced disordering defined multi-quantum well twin waveguides are shown to have similar optical properties as conventional dielectric rib waveguides. They provide a more flexible control over the waveguiding and coupling characteristics by changing the diffusion time, the ion implant energy, the mask width, the waveguide separation, and the operating wavelength. By suitably varying these parameters, single-mode operation can be achieved, while the coupling length can be theoretically tuned from a few millimeters to a hundred meters, a difference in the order of 10^5. Impurity induced disordering produced waveguide arrays are therefore highly recommended for integrated photonic IC realisation.

Keywords: waveguide couplers, ion implantation, semiconductor waveguides, quantum well devices, diffusion process

1. INTRODUCTION

The selective disordering (or otherwise known as intermixing) of III-V compound semiconductor material quantum well (QW) structures has been widely employed to realise various optoelectronics devices.[1] This technique offers a planar technology to alter the band-gap energy, refractive index and other optical properties of the QW material. Impurity-induced disordering (IID) by diffusion [2] or by ion implantation,[3] as well as impurity-free vacancy diffusion [4] can enhance the interdiffusion rate of the diffused quantum well by large extents. In this work, ion implantation is used because it provides an accurate depth control of the disordered region due to a controllable spatial distribution of ions, though it unavoidably causes some damage.

In recent years, multi-QW waveguides and their applications have aroused much interest in the optoelectronics field. Optical directional couplers, also termed waveguide couplers or coupled waveguides, are important components of optoelectronic integrated circuits. Directional couplers are primarily used as optical power splitters, switches, wavelength and polarisation (de)multiplexers. [5] The basic configuration of waveguide couplers is composed of two adjacent waveguides with a finite separation such that the guided waves in the two individual guides have an appropriate overlap that couples the two. This tunnelling of waves leads to power (energy) transfer from one waveguide to the other while light propagates along the waveguides. [6] The analysis of parallel waveguides can be performed either by expressing the coupling of energy between individual guides (coupled-mode approach) [7] or by directly analysing a structure consisting of all the guides and their surrounding media (normal-mode approach). [8] For optimum design of such devices, the propagation characteristics, namely the modal behaviour, of the analyse coupled structure have to be determined. As waveguides in practice are often made by diffusion, the channels are having arbitrary refractive index profiles (typically Gaussian or complementary error function). [9] Analytical solution to the wave equation cannot be obtained easily; therefore, numerical analysis becomes essential. A number of numerical methods have been developed to solve for the modal indices and field profiles of the guided modes of the coupled system with arbitrary cross-section and/or index profile. Examples include the effective index method, [10] the spectral index method, [11] the variational method, [12] the equipartition method, [13] the Rayleigh quotient method, [14] semivectorial finite difference method, [15] vectorial integrated finite difference method, [16] the Fourier decomposition method, [17] and the Galerkin method. [18] A review of numerical methods for the analysis of optical waveguides is available in. [19] Much work has also been done to find the exact analytic solutions for the electric field of TE modes in various structures in terms of Jacobian elliptic functions. [20]

Although there have been a great number of studies on coupled waveguides, most of them are dealing with dielectric rib waveguides and relatively few are concerned with the coupling properties in multi-quantum well twin waveguides. [21] The present study is the first of such, addressing the coupling properties of multi-quantum well twin waveguides defined by IID. A model for the ion-implanted symmetrical twin waveguide consisting of AlGaAs/GaAs MQWs is developed. By adopting a quasi-vector method based on the Finite difference method which is applied to mapped infinite domains, [22] the coupled structure is analysed. This method is accurate down to and including modal cutoff. A range of IID waveguide parameters will be examined. These include the ion implantation energy, the operating wavelength, the mask width and the waveguide separation, and both the waveguiding and coupling properties at different diffusion times. In Section II of this paper, the modeling and mathematical formulations for the twin waveguide structure are described. Numerical results are presented in Section III. Conclusions will be given in Section IV.

2. MODEL

Masked ion implantation technique is used to alter the band-gap and hence the refractive index of the as-grown square quantum well (SQW) material in selective regions. The non-implanted (mask-covered) area has higher refractive indices than the implanted (uncovered) area, thus producing lateral confinement for light. A two-dimensional single-channel waveguide is formed. [23]

The schematic of the waveguiding structure to be analysed is shown in Fig. 1. It is composed of AlGaAs/GaAs multi-quantum well layers on a thick AlGaAs buffer grown on a GaAs substrate. Two identical masks are placed side by side on the top and the whole structure is exposed in air. Both the air above and AlGaAs below the MQW layers have lower refractive index than the MQWs. Ga^+ impurity ions are injected at high energy, followed by annealing at 950°C. Two parallel and symmetric waveguides are fabricated as a consequence. The refractive index of this structure is inhomogeneous and anisotropic.

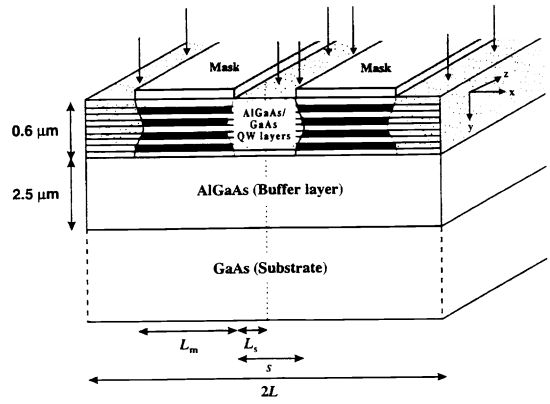

Fig. 1. Schematic of the multi-quantum well twin waveguide defined by ion implantation.

Assuming the mask has an infinitely steep edge and is thick enough to avoid penetration, the as-implanted impurity concentration profile is given by

$$N(x,y)=\frac{N_0}{\sqrt{2\pi}\Delta R_p}\exp\left[-\frac{(y-R_p)^2}{2\Delta R_p{}^2}\right]\times\frac{1}{2}\left[erfc\left(\frac{x+L_s}{\sqrt{2\Delta}R_{pL}}\right)-erfc\left(\frac{x-L_s}{\sqrt{2\Delta}R_{pL}}\right)\right.$$
$$+erfc\left(\frac{x+L}{\sqrt{2\Delta}R_{pL}}\right)-erfc\left(\frac{x-L}{\sqrt{2\Delta}R_{pL}}\right) \quad (1)$$
$$\left.+erfc\left(\frac{x-(L_m+L_s)}{\sqrt{2\Delta}R_{pL}}\right)-erfc\left(\frac{x-(L_m+L_s)}{\sqrt{2\Delta}R_{pL}}\right)\right]$$

where N_o is the implanted dose of Ga, L_m is the mask width, $2L$ is the total width of the coupled waveguide, L_s is one half of the separation between the waveguides, s (= $2L_s$) is the waveguide separation (see Fig. 1), R_p is the projected range, ΔR_p, is its vertical standard deviation and ΔR_{pL} is the lateral deviation. x is defined as the lateral direction of the waveguide and y is the depth perpendicular to it. The zero reference is at the middle and on the surface of the whole structure.

For the diffusion of impurity under annealing at a specific temperature, the diffusion coefficient D_{imp} is assumed fixed throughout the sample for any time t. The impurity concentration profile $N(x,y,t)$ can be solved from the heat equation

$$\frac{\partial N(x,y,t)}{\partial t}=D_{imp}\nabla^2 N(x,y,t) \quad (2)$$

It is assumed that the interdiffusion coefficient D_{atom} of Al and Ga atoms depends on the local defect density only, and is described by the relation

$$D_{atom}(x,y,t)=\alpha D_{imp}N(x,y,t) \quad (3)$$

where α is a constant determined from experimental data.

The square of the diffusion length $L_d{}^2(x,y)$ can be calculated by integrating $N(x,y,t)$ with respect to time,

$$L_d{}^2(x,y)=\int_0^T D_{atom}(x,y,t)dt=\alpha D_{imp}\int_0^T N(x,y,t)dt \quad (4)$$

where T is the annealing time.

The concentration profile $C(x,y,t)$of the Al atom is obtained numerically from

$$\frac{\partial C(x,y,t)}{\partial t}=\nabla(D_{atom}(x,y,t)\nabla C(x,y,t)) \quad (5)$$

Now that the diffusion length profile has much more grid points in the y direction than the number of QWs, the profile is re-gridded so that each region covers a single QW, and the mean value in each region is chosen. In this way each QW is matched with a specific diffusion length (L_d). The Al concentration profile $w(y)$ of a single QW with well width L_z is given by [24]

$$w(y)=w_0\left(1-\frac{1}{2}\left[erf\left(\frac{L_z+2y}{4L_d}\right)+erf\left(\frac{L_z-2y}{4L_d}\right)\right]\right) \quad (6)$$

where w_o is the initial Al concentration. A previously developed model [25] is adopted to find the refractive index profile $n_r(x,y)$ from the diffused QW structure.

In order to analyse the guiding characteristics of the twin waveguide, the wave equation has to be solved numerically. A semi-vector solution is required which takes into account the polarisation effects. Assuming a time dependence of $\exp(j\beta t)$ and propagation in the z-direction, for a translationally invariant real refractive index profile $n_r(x,y)$, the electric field can be described by this vector wave equation [26]

$$\nabla^2 E(x,y) + k^2 n_r{}^2(x,y) E(x,y) + \nabla\left[E(x,y) \cdot \frac{\nabla n_r{}^2(x,y)}{n_r{}^2(x,y)} \right] = 0 \tag{7}$$

where k (= $2\pi/\lambda$) is the free-space wavenumber, whereas λ represents the free-space wavelength. Considering only the transverse electric field components (E_x and E_y), propagation in the z-direction with phase change exp(-$j\beta z$) (β is the associated propagation constant), Eq. (7) reduces to two coupled equations for E_x and E_y

$$\frac{\partial^2 E_x}{\partial x^2} + \frac{\partial^2 E_x}{\partial y^2} + k^2 (n_r^2 - n_{eff}^2) E_x + 2\frac{\partial}{\partial x}\left[E_x \frac{\partial}{\partial x}\ln(n_r) + E_y \frac{\partial}{\partial y}\ln(n_r) \right] = 0 \tag{8}$$

$$\frac{\partial^2 E_y}{\partial x^2} + \frac{\partial^2 E_y}{\partial y^2} + k^2 (n_r^2 - n_{eff}^2) E_y + 2\frac{\partial}{\partial y}\left[E_y \frac{\partial}{\partial y}\ln(n_r) + E_x \frac{\partial}{\partial x}\ln(n_r) \right] = 0 \tag{9}$$

where n_{eff} (=β/k) is the modal index. The first three terms in Eq. (8) and Eq. (9) represent the scalar wave equation, the fourth term is a polarisation correction, while the last term corresponds to the coupling between E_x and E_y. For quasi-TE polarisation, $E_y = 0$. For quasi-TM polarisation, $E_x = 0$. In this paper, only the case with quasi-TE polarisation is treated. The wave equation to be solved is

$$\frac{\partial^2 E_x}{\partial x^2} + \frac{\partial^2 E_x}{\partial y^2} + k^2 (n_r^2 - n_{eff}^2) E_x + 2\frac{\partial}{\partial x}\left[E_x \frac{\partial}{\partial x}\ln(n_r) \right] = 0 \tag{10}$$

The whole infinite x-y plane was mapped onto a unit square in the u-v space using non-linear transformation functions, then E_x is expressed as a complete set of orthonormal, sinusoidal basis functions. After proper manipulations, the wave equation is finally transformed into a matrix equation. The standard eigenvalue solver - LAPACK routines - are used to solve this matrix problem. All the relevant details are described in 22.

For a given refractive index profile, $n_r(x, y)$, the normalised propagation constant b is calculated by

$$b^2 = \frac{n_{eff}{}^2 - n_{cl}{}^2}{n_{co}{}^2 - n_{cl}{}^2} \tag{11}$$

where n_{cl} and n_{co} are the refractive index of the cladding and core respectively.

Once the modal indices and guided fields of the supermodes are obtained, the coupling characteristics of the waveguide coupler can be found. This is based on the normal-mode method. The propagating electric field E at a distance z from the input can be approximated by the superposition of the supermodes of the two individual waveguides, and is represented by

$$E = c_1 E_1 e^{-jkn_e z} + c_2 E_2 e^{-jkn_o z} \tag{12}$$

where E_1 and E_2 are the fundamental even (symmetric) and the first-order odd (asymmetric) supermodes for a given polarisation, their corresponding modal indices being n_e and n_o, and their projection components of incident light being c_1 and c_2 respectively.

Two figures of merits" are commonly used in the analysis of the coupling phenomenon - the coupling coefficient κ and the coupling length L_c. The coupling coefficient describes the overlap of the individual waveguide modes, which has a larger value for more overlapping. It can be obtained by [27]

$$\kappa = \frac{\beta_e - \beta_o}{2} \tag{13}$$

where β_e and β_o are the propagation constants of the lowest-order even and odd modes respectively. The coupling length L_c is the shortest distance required for complete power transfer between two waveguides. L_c has much influence on the device length, and it is given by [28]

$$L_c = \frac{\pi}{\beta_e - \beta_o} \tag{14}$$

or by [29]

$$L_c = \frac{\lambda}{2(n_e - n_o)} \tag{15}$$

Clearly, κ and L_c have an inverse relationship. Eq. (15) is used in this study.

3. NUMERICAL RESULTS AND DISCUSSIONS

The twin waveguide structures with different geometric and optical parameters are investigated. All calculations are restricted to quasi-TE mode. Parameters to be analysed include: implant energy of the ions (600, 800 and 1000 keV), operating wavelength (0.85 and 0.90 μm), mask width (1.8, 2.4, 3 and 3.6 μm) and waveguide separation (1, 2, 3 and 4 μm). All the other parameters are kept constant: the total lateral width $2L$ is fixed at 16 μm; the thickness of MQW layers is 0.6 μm, which consists of 30 periodic layers of 100Å GaAs wells and 100Å $Al_{0.3}Ga_{0.7}As$ barriers; this is followed by a 2.5 μm thick $Al_{0.3}Ga_{0.7}As$ buffer on top of a GaAs substrate. The implant dose (N_0) is fixed at 1×10^{12} cm^{-2}, and implantation is performed at room temperature. All the waveguide structures are decomposed into a computational grid size of Δx=0.02 μm and Δy=0.002 μm, these totaled 400 and 500 grid points in the x and y directions respectively. Each implant energy is associated with a specific projected range R_p, projected standard deviation ΔR_p, and lateral spread ΔR_{pL}.[30] These values are listed in Table 1. Fig. 2 shows the Ga^+ ion impurity concentration profile when the implant energy is 600 keV, over a mask width of 3 μm, and a waveguide separation of 4 μm. For the computation of Al concentration profile post implantation, the time step dt is taken to be 0.002s in Eq. (5). To solve for the wave equation (Eq. (10)), the modal electric field is expanded in Fouries series using 30 harmonics in both x and y directions in a mapped unit square u-v space, which gives rise to a 900 × 900 matrix.

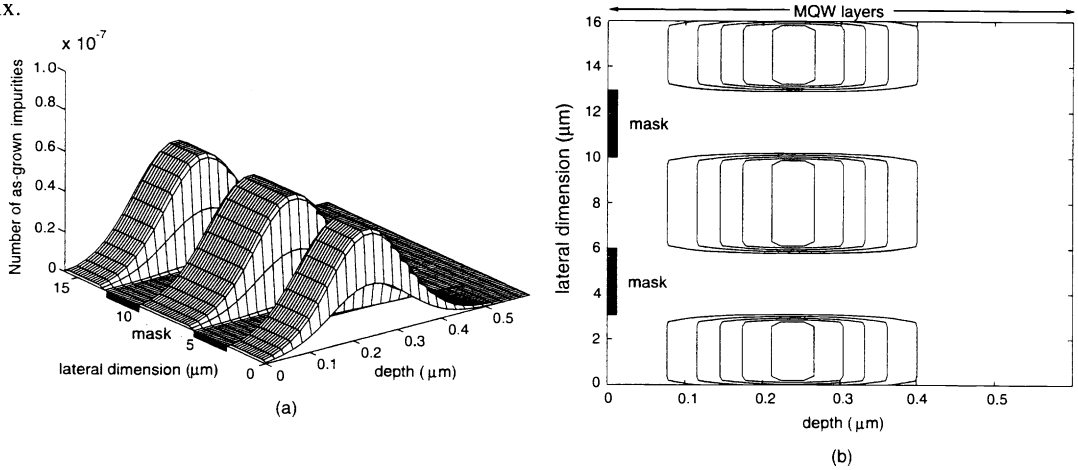

Fig. 2 Impurity concentration profile. (a) 3-D plot; (b) contour plot, with implant energy = 600 keV, mask width L_m = 3 μm, and waveguide separation s = 4 μm.

Implant energy (keV)	Projected range R_p (μm)	Vertical deviation ΔR_p (μm)	Lateral deviation ΔR_{pL} (μm)
600	0.2308	0.855	0.1081
800	0.3111	0.1069	0.1383
1000	0.3916	0.1261	0.1665

Table 1 Project range, its vertical and lateral deviation associated with different implant energies for Ga^+ implantation on AlGaAs/GaAs.

The guided modes in a two-channel waveguide are the two lowest-order symmetric and asymmetric supermodes. Their normalised propagation constant, b (defined in Eq. (11)), are referred to as b_e and b_o, both indicating how far a mode is from cutoff. They are the normalised values of β_e and β_o (appeared in Eq. (14)) respectively. b_e and b_o are found out to be very close, differed by much less than 10^{-3} in most cases. b_e is always larger than b_o, which conforms the fact that the coupling length must be positive. The two b values both increase as diffusion time proceeds. As the two waveguides are in proximity, coupling occurs between them. While various physical parameters of the waveguide structure is changed, the degree of coupling in each case is measured by the coupling length L_c using Eq. (15).

3.1 Symmetric Dual-channel Waveguide

The waveguide structure produced at ion implant energy equals 1000 keV, with mask width equals 1.8 μm, and operating wavelength at 0.90 μm is taken as a typical case for illustrating the results with symmetric waveguide. High energy ion implantation has been employed recently for bandgap tuning of semiconductor quantum well laser structures. [31] Considering the effect of waveguide separation, it is discovered that for all waveguide separations under investigation, diffusion time t = 36 s marks the beginning of guided modes and single-mode operation is still maintained up to t = 100s. b_e and b_o are very similar in value. Table 2 shows the values of n_e and n_o at different diffusion time for different waveguide separations. Apparently the waveguide separation has a minimal effect on the modal indices (also the propagation constants), in consideration of the fact that the corresponding values of n_e or n_o for different waveguide separations are almost the same. It also does not affect the time of occurrence of guided modes and the time duration of single-mode operation.

Diffusion	s = 1 (mm)		s = 2 (mm)		s = 3 (mm)		s = 4 (mm)	
time (s)	n_o	n_e	n_o	n_e	n_o	n_e	n_o	n_e
36	3.470467	3.470556	3.470508	3.470511	3.470511	3.470511	3.470509	3.470509
60	3.469368	3.469416	3.469385	3.469386	3.469391	3.469391	3.469385	3.469385
100	3.468025	3.468050	3.468035	3.468036	3.468037	3.468037	3.468034	3.468034

Table 2 Even and odd modal indices n_e and n_o at different diffusion time for different waveguide separations s, with implant energy = 1000 keV, mask width L_m = 1.8 mm, and operating wavelength l_{op} = 0.90 mm.

It is evident that for small waveguide separation, there is a relatively large difference between the modal indices of the lowest-order even and odd supermodes guided by the twin waveguide. When the separation increases, their difference decreases and they both tend to that of the fundamental mode of a single guide. (The same result is reported in [32].) Since the coupling length is inversely related to this difference, the coupling length becomes longer as the waveguide separation increases. This is expected because the interaction between the guides naturally gets smaller as they are farther apart, giving rise to a smaller coupling coefficient and hence a longer coupling length. Table 3 shows the theoretical calculated values of L_c in this case, which are shown graphically in Fig. 3 using a logarithmic scale. L_c varies greatly from a few millimeters to a hundred meters. The exceptionally large values of L_c for large waveguide separations are unrealistic since they are too large to be employed in real devices. They also imply that there is practically no coupling.

Diffusion	s =1 (mm)	s = 2 (mm)	s = 3 (mm)	s = 4 (mm)
time (s)	L_c	L_c	L_c	L_c
36	0.0051	0.1497	4.0120	8.6927
60	0.0095	0.4274	8.9305	27.1247
100	0.0183	1.3407	74.5967	81.9981

Table 3 Coupling length L_c at different diffusion time for different waveguide separations s, with implant energy = 1000 keV, mask width L_m = 1.8 mm, and operating wavelength l_{op} = 0.90 mm.

As diffusion proceeds (diffusion time $t > 36$ s), the coupling length rises, as shown in Fig. 3. This may be explained by the fact that Δn_r, the difference in the refractive indices in the implanted and non-implanted regions, gets larger, thus producing a stronger optical confinement effect. This implies less light can propagate into the adjacent channel. It can therefore be concluded that guiding improves while the extent of coupling decreases with diffusion time. Moreover, the coupling length corresponding to larger waveguide separations experiences a more rapid increase than that for smaller separations (this is represented by the slope of the L_c curves.) This can be explained as follows. There is a weak coupling at the beginning of guided modes for large waveguide separations, so it is easier to "decouple" the fields from the two guides. In fact, "decoupling" means reducing the overlapping between the fields from the two guides (or the coupling coefficient). This is accompanied by a longer coupling length. By contrast, there is more coupling at the beginning of guided modes for small waveguide separations. To decouple the two guides, it would require a longer diffusion time.

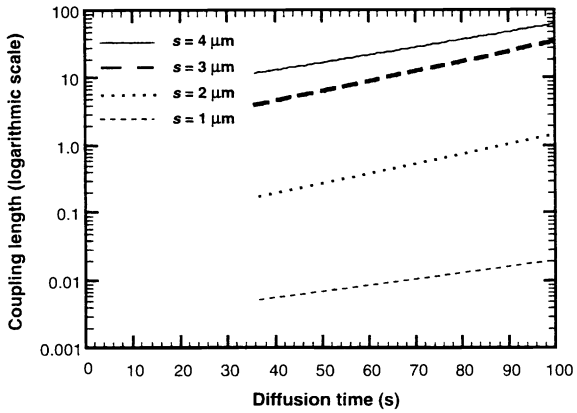

Fig. 3 Coupling length L_c versus diffusion time for different waveguide separations s, implant energy = 1000 keV, mask width L_m = 1.8 μm, and operating wavelength λ_{op} = 0.90 μm.

If the operating wavelength λ_{op} is changed to 0.85 μm, a different set of coupling lengths under single mode operation is obtained (see Table 4). For shorter wavelengths, guided modes will occur earlier but single-mode operation will last for a shorter time. The trend for coupling length versus time is the same as that observed for λ_{op} = 0.90 μm. Comparing the values of coupling length when guided modes have just begun, it is found that coupling length is smaller for longer wavelength, which suggests that the degree of coupling is greater for longer wavelengths.

Diffusion time (s)	s =1 (mm) L_c	s = 2 (mm) L_c	s = 3 (mm) L_c	s = 4 (mm) L_c
6	0.0053	0.1690	7.5794	9.1936
8	0.0084	0.3737	48.6159	59.5110
10	0.0121	0.7119	77.0969	107.1463

Table 4 Coupling length L_c at different diffusion time for different waveguide separations s, with implant energy = 1000 keV, mask width L_m = 1.8 mm, and operating wavelength l_{op} = 0.85 mm.

The coupling phenomenon can also be visualised from the contour plot of the quasi-TE modal field profiles. In general, the contour plots of the leading even modal fields show a considerably larger overlapping of the fields from the two guides than those of the odd modal fields. Comparing the field profiles observed at an operating wavelength of 0.90 μm and

that at 0.85 μm, it can be seen that for the same waveguide structure, the profiles belonged to longer wavelength experience greater vertical spreads than their shorter wavelength counterparts.

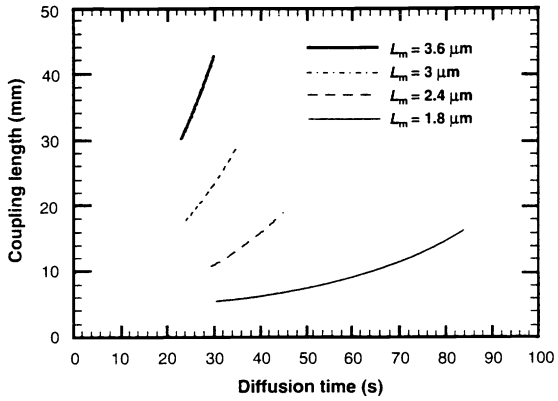

Fig. 4 Coupling length L_c versus diffusion time for different mask widths L_m, implant energy = 800 keV, waveguide separation s = 1 μm, and operating wavelength λ_{op} = 0.90 μm.

The relationship between mask width and coupling length is now investigated. Fig. 4 shows the coupling length against diffusion time for different mask widths at an operating wavelength of 0.90 μm. The implant energy is 800 keV, and the waveguide separation is 1 μm. In short, the wider the mask, the longer the coupling length. This is obvious as light is confined better in a larger region under larger masks. Hence, the degree of coupling is smaller. As before, the slope for curves corresponding to weaker coupling (larger mask width in this case) is greater, as explained earlier. Fig. 5 are the field contour plots for mask widths equal to 2.4 and 3.6 μm. It turns out that the diffusion time for guided modes to occur as well as the time duration for single-mode operation decreases with increasing mask width. It implies that to shorten the diffusion time, a wider mask is desirable; however, the undesirable multi-mode guiding will occur earlier.

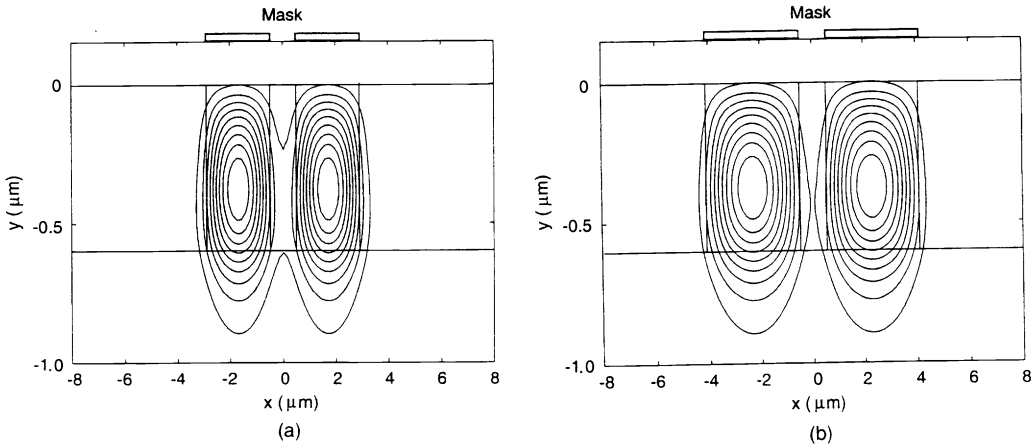

Fig. 5 Contour plots of the lowest-order even modal field for to different mask widths. (a) L_m = 2.4 μm; (b) L_m = 3.6 μm, with implant energy = 600 keV, waveguide separation s = 1 μm, and operating wavelength λ_{op} = 0.90 μm.

Finally, the influence of implant energy on the coupling length is investigated. Lower implant energies are observed to shorten the coupling length. Fig. 6 shows the coupling length against diffusion time for different implant energies where the operating wavelength is 0.90 μm, mask width is 1.8 μm and waveguide separation is 1 μm. Other things being constant, greater implant energies will require longer diffusion time for guided modes to occur, and the time duration for single-mode operation is longer.

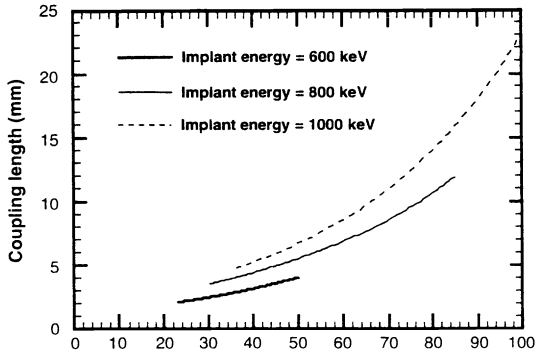

Fig. 6 Coupling length L_c versus diffusion time for different implant energies, with mask width L_m = 1.8 μm, waveguide separation s = 1 μm, and operating wavelength λ_{op} = 0.90 μm.

There is one remark about the coupling length L_c. As seen from Eq. (14) and Eq. (15), L_c is inversely proportional to the difference between the even and odd propagation constants β_e and β_o or the modal indices n_e and n_o. Small errors in any one parameter will produce large errors in L_c. The calculation of L_c usually requires an accuracy of about 1 part to 10^5 in the calculated modal propagation constants and indices 29. This is guaranteed in our method. However, when the separation between the two adjacent guides gets larger, the difference between theses even and odd parameters will be smaller. The accuracy in L_c will decrease due to the subtraction error.

3.2 Asymmetric Dual-channel Waveguide

Attention is now turned to asymmetric dual-channel waveguide couplers. All physical dimensions and grid sizing are the same as before, but this time one of the masks is having a fixed width (L_{m1} = 2.4 μm); the other mask has a variable width, L_{m2}. The calculations are also restricted to the quasi-TE modes. The case where implant energy is 600 keV, waveguide separation is 1 μm with operating wavelength at 0.90 μm is chosen to be discussed here.

As L_{m2} is varied, the modal indices of the two lowest-order supermodes behave differently. When L_{m2} is smaller than L_{m1} , the modal index of the even supermode approaches to that of the fundamental mode of the isolated guide with wider mask width L_{m1}; when L_{m2} is larger than L_{m1}, it approaches to that of an isolated guide of mask width L_{m2}. By contrast, when L_{m2} is larger than L_{m1}, the modal index of the odd supermode approaches to that of the fundamental mode of the isolated guide with smaller mask width L_{m1}; when L_{m2} is smaller than L_{m1}, it approaches to that of an isolated guide of mask width L_{m2}. The difference between the modal indices of the even and odd supermodes is minimum for symmetric couplers (when $L_{m2} = L_{m1}$ = 2.4 μm), as assumed by the coupled-mode theory. These trends are illustrated in Fig. 7, which suggest that the even and odd supermodes are distributed unequally between the two waveguides. The even mode is mainly guided by the larger guide (the one with larger mask width), while the odd supermode is mainly guided by the smaller guide (the one with smaller mask width).

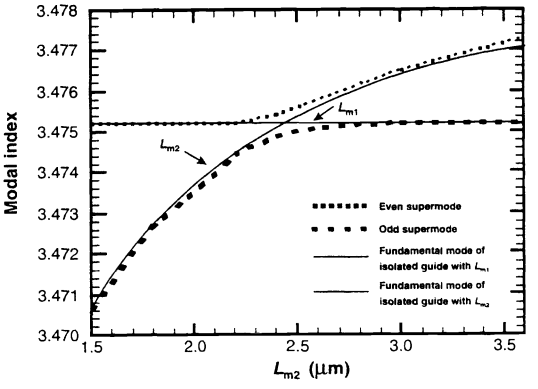

Fig. 7 Modal index of the two lowest-order supermodes and the fundamental mode of the isolated waveguides as a function of mask width L_{m2} with implant energy = 600 keV, mask width L_{m1} = 2.4 μm, waveguide separation s = 1 μm, and operating wavelength λ_{op} = 0.90 μm.

To study the effect of asymmetry on the coupling properties, the normalized power transferred between the two channels for different mask width L_{m2} are compared. The method for determining the power transfer from one waveguide to another is available in [33]. It is found that power transfer between symmetric waveguides is complete, while that between asymmetric waveguides is only partial and decreases as the asymmetry increases, as evident in Fig. 10. It should be noticed that for the same difference of $|L_{m2} - L_{m1}|$, the power transferred when L_{m2} is smaller L_{m1} is greater than that when L_{m2} is larger L_{m1} (that is to compare the values of power transferred for L_{m2} = 1.8 μm and L_{m2} = 3 μm). This phenomenon is because smaller mask width contributes to weaker optical confinement effect; the modal fields are more diffused such that they exchange energy to a greater extent.

4. CONCLUSIONS

A model has been developed for studying symmetric and asymmetric multi-QW directional couplers defined by the ion implantation technique. It enables a quasi-vector analysis of the light propagation for various IID waveguide structures. Knowledge of the modal indices and field profiles of the supermodes, and the coupling length, has been gathered to facilitate the design of IID defined integrated optoelectronic devices.

The effects of the implantation and geometric parameters on the waveguiding and coupling properties of the dual-core waveguide structures are analysed. The time of occurrence of the first guided modes and the time duration of single-mode operation do not vary with the twin waveguide separation. They tend to decrease with smaller implant energy, wider mask width and shorter operating wavelength. By choosing these parameters appropriately, the number of guided modes can be controlled and single-mode propagation can be achieved in the twin waveguide structure. In regard to the coupling characteristics of the coupled waveguide structure, the coupling length is shorter with smaller waveguide separation, longer operating wavelength, smaller mask width, and smaller implant energy. Shorter coupling length (or larger coupling coefficient in equivalent) means greater overlapping of the guided fields of the adjacent waveguides. One very important finding is that the coupling length increases with diffusion time.

This study shows that while IID produced multi-QW twin waveguides possess similar optical properties compared with conventional dielectric rib waveguides, they have the advantage of providing a more flexible control over the waveguiding and coupling characteristics, such as by varying the diffusion time, the ion implant energy, the mask width, the waveguide separation, and the operating wavelength. Therefore IID produced waveguide arrays are highly recommended for integrated photonic IC realisation. The IID technique permits the fabrication of directional couplers of various types at different sections of the waveguide arrays through selective intermixing in selective areas, thus eliminating the need of waveguide bending or junction.

A possible future extension of our work is to deal with multi-channel (eight- and sixteen-channel) waveguiding structures. These multi-port devices are becoming today's major focus in WDM (wavelength division multiplexing) applications.

5. ACKNOWLEDGEMENT

The author would like to thank Steve Y. T. Wong for their valuable technical assistance and helpful discussions. This paper is supported by the Hong Kong RGC earmarked grant and the University of Hong Kong CRCG grant.

6. REFERENCES

1. B.L. Weiss, Ed., "Special Issue on Quantum Well Mixing for Optoelectronics," *Opt. Quantum Electron.*, vol. 23, pp. S799-S994, 1991; E.H. Li, Ed., "Semiconductor Quantum Well Intermixing," Langhorne: Gordon & Breach, 1997.
2. D.G. Deppe and N. Holonyak, Jr., "Atom diffusion and impurity-induced layer disordering in quantum well III-V semiconductor heterostructure," *J. Appl. Phys.*, vol. 64, pp. R93-R113, 1988.
3. I. Harrison, "Impurity-induced disordering in III-V multi-quantum well and superlattices," *J. Mat. Sci.: Mat. in Electron.*, vol. 4, pp. 1-28, 1993.
4. J.H. Marsh, "Quantum well intermixing," *Semicond. Sci. Technol.*, vol. 8, pp. 1136-1155, 1993.
5. C.F. Janz, B.P. Keyworth, W. Allegretto, R.I. MacDonald, M. Fallahi, G. Hillier, and C. Rolland, "Mach-Zehnder switch using an ultra-compact directional coupler in a strongly-confining rib structure," *IEEE Photon. Technol. Lett.*, vol. 6, pp. 981-983, 1994.
6. R.Q. Yang, "Electron transfer efficiency in quantum well waveguide couplers," *J. Appl. Phys.*, vol. 80, pp. 1541-1546, 1996.
7. H.A. Haus, W.P. Huang, S. Kawakami, and N.A. Whitaker, "Coupled-mode theory of optical waveguides," *J. Lightwave Tech.*, vol. LT-5, pp. 16-23, 1987.
8. E. Marom, O.G. Ramer, and S. Ruschin, "Relation between normal-mode and coupled-mode analyses of parallel waveguides," *IEEE J. Quant. Electron.*, vol. QE-20, pp. 1311-1319, 1984.
9. R.K. Lagu and R.V. Ramaswamy, "A variational finite-difference method for analyzing channel waveguides with arbitrary index profiles," *IEEE J. Quant. Electron.*, vol. QE-22, pp. 968-976, 1986.
10. J. Buus, "The effective index method and its application to semiconductor lasers," *IEEE J. Quant. Electron.*, vol. QE-18, pp. 1083-1089, 1982.
11. S.V. Burke, "Spectral index method applied to rib and strip-loaded directional couplers," *IEE Proc.*, vol. 137, pp. 7-10, 1990.
12. W.P. Huang and H.A. Haus, "A simple variation approach to optical rib waveguides," *J. Lightwave Tech.*, vol. 9, pp. 56-61, 1991.
13. T.M. Benson and P.C. Kendall, "Equipartition method for the analysis of two nonidentical closely separated rib waveguides," *IEE Proc. J.*, vol. 140, pp. 62-65, 1993.
14. M.S. Stern, "Rayleigh quotient solution of semivectorial field problems for optical waveguides with arbitrary index profiles," *IEE Proc. J.*, vol. 138, pp. 185-190, 1991.
15. M.S. Stern, "Semivectorial polarized finite difference method for optical waveguides with arbitrary index profiles," *IEE Proc.*, vol. 135, pp. 56-63, 1988.
16. H. Dong, J. Zou, and A. Gopinath, "Vectorial integrated finite-difference analysis of dielectric waveguides," *J. Lightwave Tech.*, vol. 11, pp. 1559-1563, 1993.
17. S. J. Hewlett and F. Ladouceur, "Fourier decomposition method applied to mapped infinite domains: scalar analysis of dielectric waveguides down to modal cutoff," *J. Lightwave Tech.*, vol. 13, pp. 375-383, 1995.
18. D. Marcuse, "Solution of the vector wave equation for general dielectric waveguides by the Galerkin method," *IEEE J. Quant. Electron.*, vol. 28, pp. 459-465, 1992.
19. K.S. Chiang, "Review of numerical and approximate methods for the modal analysis of general optical dielectric waveguides," *Opt. Quantum Electron.*, vol. 26, pp. S113-S134, 1994.
20. J. D. Begin and M. Cada, "Exact analytic solutions to the nonlinear wave equation for a saturable Kerr-like medium: modes of nonlinear optical waveguides and couplers," *IEEE Trans.*, vol. 30, pp. 3006-3016, 1994.

21. C. Ma, "Coupling properties in periodic waveguides and in multiple quantum-well waveguides," *IEEE J. Quant. Electron,* vol. 30, pp. 2811-2816, 1994.
22. K.M. Lo and E. H. Li, "Gelerkin's method applied to mapped infinite domains: quasi-vector solutions for optical waveguide modes," in *Proc. Optoelectronics and Communications Conference (OECC '96), Chiba, Japan,* pp. 430-431, 1996.
23. T. Wolf, C.L. Shieh, R. Engelmann, K. Alavi, and J. Mantz, "Lateral refractive index step in GaAs/ AlGaAs multiple quantum well waveguides fabricated by impurity-induced disordering," *Appl. Phys. Lett.,* vol. 55, pp. 1412-1414, 1989.
24. E. H. Li and B.L. Weiss, "Exciton optical absorption in a diffusion induced non-square AlGaAs/GaAs quantum well," *Quantum Well and Superlattice Physics IV,* SPIE vol. 1675, pp. 98-104, 1992.
25. E.H. Li, B.L. Weiss, K.S. Chan, and J. Micallef, "Polarization dependent refractive index of an interdiffusion induced AlGaAs/GaAs quantum well," *Appl. Phys. Lett.* Vol. 62, pp. 550-552, 1993.
26. A. Weisshaar, J. Li, R.L. Gallawa, and I.C. Goyal, "Vector and quasi-vector solutions for optical waveguide modes using efficient Galerkin's method with Hermite-Gauss basis functions," *J. Lightwave Tech.,* vol. 13, pp. 1795-1800, 1995.
27. A. Hardy and W. Streifer, "Coupled mode theory of parallel waveguides," *J. Lightwave Tech.*, vol. LT-3, pp. 1135-1146, 1985.
28. Z. Mao and W.P. Huang, "Analysis of optical rib waveguides and couplers with buried guiding layer," *IEEE J. Quant. Electron.*, vol. 28, pp. 176-183, 1992.
29. C.H. Henry and B.H. Verbeek, "Solution of the scalar wave equation for arbitrary shaped dielectric waveguides by two-dimensional Fourier analysis," *J. Lightwave Tech.*, vol. 7, pp. 308-313, 1989.
30. F. Gibbons, W.S. Johnson, and S.W. Mylroie, "Range statistics in semiconductors," Academic, New York, 1975.
31. S. Charbonneau, P.J. Poole, P.G. Piva, M. Buchanan, R.D. Goldberg, I.V. Mitchell, "Bandgap tuning of semiconductor quantum well laser structures using high energy ion implantations," *Nucl. Instrum. Meth. B*, vol. 106, pp. 457-460, 1995.
32. J.Y. Su, P.K. Wei, and W.S. Wang, "A new iterative method for the analysis of longitudinally invariant waveguide couplers," *J. Lightwave Tech.*, vol. 12, pp. 2056-2065, 1994.
33. M.D. Feit and Fleck, Jr., J.A., "Propagating beam theory of optical fiber cross coupling," *IEEE J. on selected areas in communications*, vol. 71, pp. 1361-1372, 1981.